Rocksalt and Layered Metal Sulfides for Li Storage Applications: Li*Me*$_{0.5}$Ti$_{0.5}$S$_2$ (*Me* = Fe^{2+}, Mn^{2+}, and Mg^{2+}).

Miyuki Shinoda,[1] Hongahally Basappa Rajendra,[2] and Naoaki Yabuuchi[1-3*]

[1]Department of Chemistry and Life Science, Yokohama National University, 79-5 Tokiwadai, Hodogaya-ku, Yokohama, Kanagawa 240-8501, Japan

[2]Advanced Chemical Energy Research Center, Institute of Advanced Sciences, Yokohama National University, 79-5 Tokiwadai, Hodogaya-ku, Yokohama, Kanagawa 240-8501, Japan

[3]Elements Strategy Initiative for Catalysts and Batteries, Kyoto University, f1-30 Goryo-Ohara, Nishikyo-ku, Kyoto 615-8245, Japan.

KEYWORDS metal sulfide, anionic redox, rocksalt sulfides, lithium battery, polymer battery

ABSTRACT: Lithium containing metal sulfides, Li*Me*$_{0.5}$Ti$_{0.5}$S$_2$ (*Me* = Fe^{2+}, Mn^{2+}, and Mg^{2+}) with cation-disordered rocksalt and cation-ordered layered structure, are synthesized and tested as electrode materials for Li battery applications. The disordered rocksalt sulfides show better electrode performance when compared with materials with the ordered layered structure, which is a clearly different trend from lithium containing metal oxides. Nearly all Li ions are reversibly extracted with anionic redox for rocksalt Li$_{1-x}$Mn$_{0.5}$Ti$_{0.5}$S$_2$. Although electrode reversibility is not high because of relatively higher solubility to carbonate-based electrolyte solution, cyclability as electrode materials is effectively improved by the use of polymer-based solid electrolyte.

To realize a fossil fuel free society, the market on electric vehicles equipped with Li-ion batteries is rapidly growing throughout the world. Ni-enriched layered oxides are currently used for positive electrode materials of Li-ion batteries in electric vehicles.[1-3] The cost reduction of a positive electrode material, which is the most expensive battery component for practical Li-ion batteries,[4] is necessary to further decrease the cost of batteries, leading to the further expansion of battery market. Sulfur has been extensively studied as a potential positive electrode material for Li-ion batteries.[5] However, intrinsically low electronic conductivity for sulfur requires relatively a lower sulfur loading and higher fraction of carbon in the composite electrode.[6] In contrast, metal sulfides, *e.g.*, TiS$_2$, shows high electrical conductivity, and used as highly reversible electrode materials even without the addition of conductive carbon materials.[7] Nevertheless, electrode materials without Li ions in the host structure, like TiS$_2$, cannot be used as positive electrode materials with graphite as negative electrode materials. Li-containing sulfides with transition metal ions, *e.g.*, Li$_2$TiS$_3$,[8,9] Li$_{1.33-2y/3}$Ti$^{4+}_{0.67-y/3}$Fe$^{2+}_y$S$_2$,[10] and Li$_2$FeS$_2$,[11] were studied as potential high-capacity positive electrode materials. However, reports on Li-containing transition metal sulfides are limited. In contrast, many sulfides with main group elements, *e.g.*, Li$_3$PS$_4$, Li$_{10}$GeP$_2$S$_{12}$, Li$_2$SnS$_3$ *etc.*,[12] were reported and tested as ionic conductors. These differences originate from the difference in chemical stability for transition metal and main group elements with higher oxidation states coupled with reductive characteristics of sulfide ions. For the case of oxides, LiMnO$_2$ with trivalent transition metal ions are widely studied for battery applications.[13,14] However, Mn^{3+} are easily reduced by sulfide ions, and thus, synthesis of LiMnS$_2$ is expected to be difficult. Similarly, other late-transition metal ions, like Fe^{3+}, Co^{3+}, and Ni^{3+}, requires oxidative environment for stabilization. Therefore, the synthesis of metal sulfides with these trivalent transition metal ions would be challenging. A material design concept is altered for sulfide-based electrode materials compared with well-established metal oxides.[15,16]

In this study, Fe^{2+} and Mn^{2+} ions with Ti^{4+} ions, which are chemically stable as transition metal ions under reductive environment, are targeted as potential positive electrode materials. As model electrode materials with sulfide ions, LiFe$_{0.5}$Ti$_{0.5}$S$_2$[17,18] and LiMn$_{0.5}$Ti$_{0.5}$S$_2$ are synthesized and its electrochemical reversibility is examined in Li cells. For comparison, LiMg$_{0.5}$Ti$_{0.5}$S$_2$ is also synthesized. Factors affecting electrode reversibility for metal sulfides are discussed through the comparison of electrode performance of these different electrode materials with transition metal ions.

Li*Me*$_{0.5}$Ti$_{0.5}$S$_2$ (*Me* = Fe^{2+}, Mn^{2+}, and Mg^{2+}) were synthesized from Li$_2$S, TiS$_2$, and *Me*S (*Me* = Fe^{2+}, Mn^{2+}, and Mg^{2+}) by mechanical ball milling. For instance, 0.188 g of Li$_2$S (Sigma-Aldrich) and 0.457 g of TiS$_2$ (Sigma-Aldrich), and 0.355 g of MnS (Sigma-Aldrich) were mixed using a planetary ball mill (PULVERISETTE 7; FRITSCH) with a ZrO$_2$ pot (45 mL) and balls at 600 rpm for 12 h. The samples were handled in an Ar-filled glove box to avoid the contact to moisture. Structural evolutions of the samples by milling were studied using an X-ray diffractometer (D2 PHASER, Bruker) equipped with a high-speed one-dimensional detector. As shown in X-ray diffraction (XRD) patterns (**Figure 1**), nanosized sulfides with a cation-disordered rocksalt structure are synthesized by mechanical ball milling. Low crystallinity phases, which consist of agglomerated nanosized particles, less than 10 nm, as expected from peak widths for diffraction lines, are formed by mechanical milling, which is also a common feature for the samples prepared by high-energy mechanical milling.[13,19] The presence of

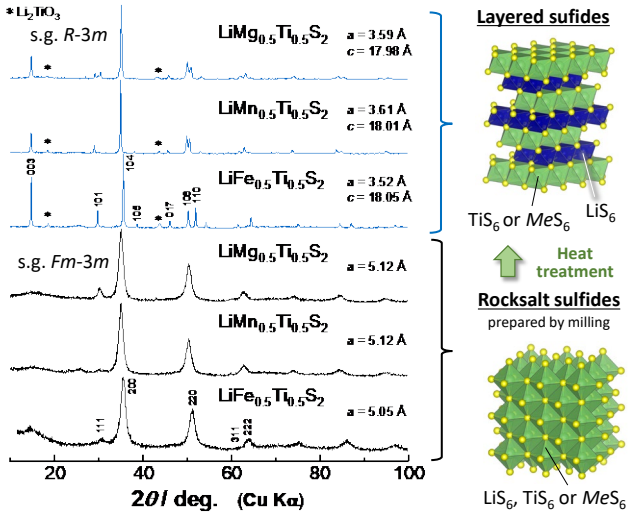

Figure 1. XRD patterns and SEM images of as-prepared and heat-treated Li*Me*$_{0.5}$Ti$_{0.5}$S$_2$ (*Me* = Fe^{2+}, Mn^{2+}, and Mg^{2+}). Schematic illustrations of crystal structures, which were drawn by using the VESTA program,[20] are also shown.

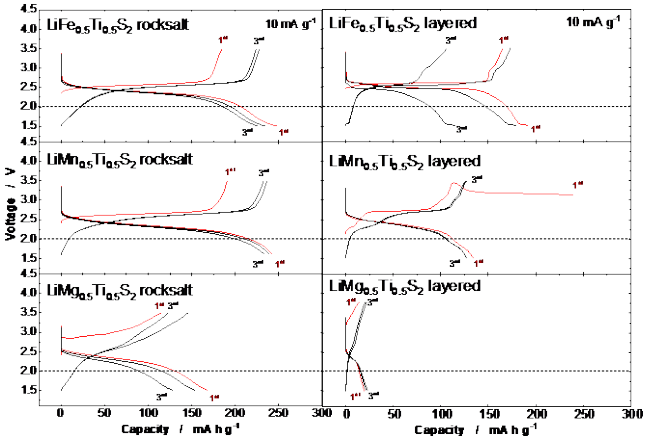

Figure 2. Galvanostatic charge/discharge curves of as-prepared and heat-treated Li*Me*$_{0.5}$Ti$_{0.5}$S$_2$ (*Me* = Fe^{2+}, Mn^{2+}, and Mg^{2+}) at a rate of 10 mA g^{-1} at room temperature. Dotted lines are guide for the eye. The highest discharge capacity above 2.0 V is obtained for rocksalt $LiMn_{0.5}Ti_{0.5}S_2$. Mass loading of metal sulfides ranges from 2.8 – 3.3 mg cm^{-2}, corresponding to density of 0.33 – 0.53 g cm^{-3}.

agglomerated nanosized particles is also confirmed by scanning electron microscopy (SEM) observation as shown in **Supporting Figure S1a**. The Brunauer-Emmett-Teller (BET) specific surface area was measured at 77 K on a micromeritics surface area and porosity analyzer (BELSORP-MINI X; Microtrac MRB). BET surface area were measured to be 15.4 m^2 g^{-1} for rocksalt $LiMn_{0.5}Ti_{0.5}S_2$ (**Supporting Figure S1b**). The agglomeration of nanosized particles is also supported from the relatively small surface area for nanosized and rocksalt $LiMn_{0.5}Ti_{0.5}S_2$.[21] These low crystallinity phases with the disordered rocksalt structure synthesized by mechanical milling are metastable phases, and therefore after heat-treatment in the glove box at 500 °C for 3 h, all samples were changed into an α-$NaFeO_2$-type layered structure. A minor impurity phase, which is assigned into Li_2TiO_3, is also found for all layered phases. A similar impurity phase was also reported in literature.[9,10] No clear change in particle morphology by heating is observed (**Supporting Figure S1**). The BET surface area is decreased to 2.0 m^2 g^{-1} for layered $LiMn_{0.5}Ti_{0.5}S_2$. Note that a thermodynamically stable phase of $LiMn_{0.5}Ti_{0.5}O_2$ crystallizes into a rocksalt structure.[22] This fact suggests that a large gap in ionic radii between cationic and anionic sites for 3d transition metal sulfides also energetically de-stabilizes disordered rocksalt structure, and thus the non-isotropic structure is formed to compensate the large size gap for both cationic and anionic sites through the structural distortion along *c*-axis direction.

Galvanostatic charge/discharge curves of Li*Me*$_{0.5}$Ti$_{0.5}$S$_2$ (*Me* = Fe^{2+}, Mn^{2+}, and Mg^{2+}) before and after heat treatment are compared in **Figure 2**. Composite positive electrodes comprised of 80 wt% Li*Me*$_{0.5}$Ti$_{0.5}$S$_2$, 10 wt% acetylene black, and 10 wt% polyvinylidene fluoride (KF 1100; Kureha Co. Ltd.) were dispersed in N-methylpyrrolidone and pasted on aluminum foil as a current collector. The electrodes were dried at 120 °C for 2 h in vacuum. Metallic lithium (Honjo Metal Co. Ltd.) was used as a negative electrode. The electrolyte solution used was 1.0 mol dm^{-3} $LiPF_6$ dissolved in ethylene carbonate/dimethyl carbonate (3:7 by volume, battery grade; Kishida Chemical Co. Ltd.). Two-electrode cells (TJ-AC; Tomcell Japan) were assembled in the Ar-filled glovebox. Rocksalt $LiFe_{0.5}Ti_{0.5}S_2$ and $LiMn_{0.5}Ti_{0.5}S_2$ deliver large reversible capacities, 240 – 250 mA h g^{-1}, and these experimentally observed reversible capacities nearly correspond to the theoretical capacity. Selected charge/discharge curves and capacity retention of both electrodes for 20 cycles is also shown in **Supporting Figure S2a** and **b**. Nearly 70% of reversible capacity is lost after 20 cycles, and inferior capacity retention originates from relatively higher solubility of sulfide-based electrode materials into carbonate-based electrolyte (Also see the result of dissolution test[23] for fully charged $Li_{1-x}Mn_{0.5}Ti_{0.5}S_2$ in **Supporting Figure S2c**), which is also discussed in the later section. In contrast to the results for the samples with Fe and Mn ions, $LiMg_{0.5}Ti_{0.5}S_2$ shows a smaller reversible capacity as electrode materials. Larger polarization on an initial charge curve is also noted. The increase in the impedance is also noted as shown in **Supporting Figure S3a**. Smaller impedance of a first semi-circle, which is influenced by the through-plane resistance of composite electrodes,[24] is noted for rocksalt $LiMn_{0.5}Ti_{0.5}S_2$. Because ionic conduction paths are identical for Li$_{1-x}$*Me*$_{0.5}$Ti$_{0.5}$S$_2$ (*Me* = Fe^{2+}, Mn^{2+}, and Mg^{2+}), the inferior electrode performance for $LiMg_{0.5}Ti_{0.5}S_2$ is expected to originate from the decreasing electronic conductivity of active materials by the substitution of Mg^{2+} ions without conductive electrons. Note that electrode reversibility is further reduced by heat treatment. Layered $LiMg_{0.5}Ti_{0.5}S_2$ is regarded as electrochemically inactive. Similar to this study, it has been reported that rocksalt and low crystallinity Li_2TiS_3 is electrochemically active,[25] but crystalline and layered Li_2TiS_3 is electrochemically inactive.[9,10] TiS_2, FeS, and MnS are good electronic conductors whereas Li_2S and MgS without transition metal ions are not good conductors. For materials with the rocksalt structure, S-shaped voltage profiles are observed and the voltage slope is larger compared with layered materials, which is triggered by structural disordering with different local environments for cationic and anionic species.[26] This fact also suggests that transition metal d and sulfur p bands would be broadened and thus would contribute the enhancement of electronic conductivity. The presence of structural defects would also contribute better conductivity for the sample with the nanosized rocksalt structure. Indeed, much smaller impedance is noted for rocksalt $LiMn_{0.5}Ti_{0.5}S_2$ compared with layered $LiMn_{0.5}Ti_{0.5}S_2$ (**Supporting Figure S3b**). These differences for cationic species (with or without d-electron orbitals) and crystal structures (order or disordered structures) influence electrode performance of sulfide-based electrode materials. The

larger surface area for rocksalt sulfides is also expected to influence the electrode reversibility. However, the improvement of electrode kinetics for layered $LiMn_{0.5}Ti_{0.5}S_2$ is not evidenced by the operation at the elevated temperature (**Supporting Figure S4**).

Reaction mechanisms have been further studied by *ex-situ* synchrotron XRD study. **Figure 3a** shows changes in synchrotron XRD patterns of rocksalt $Li_{1-x}Mn_{0.5}Ti_{0.5}S_2$. After full extraction of Li ions, a small change in unit cell volume (< 1%) without phase transitions is evidenced. In addition, lowering crystallinity after delithiation is not observed. This finding is in contrast to the observation for rocksalt Li_2TiS_3, in which the significant reduction of crystallinity and amorphous phase formation are evidenced after full delithiation.[25] Note that a peak shift to lower diffraction angle and the reduction of unit cell volume is observed for $Li_{1-x}Fe_{0.5}Ti_{0.5}S_2$ and $Li_{1-x}Mg_{0.5}Ti_{0.5}S_2$ (**Supporting Figure S5** and **S6**). Such small volume change is only found for $Li_{1-x}Mn_{0.5}Ti_{0.5}S_2$ among three samples.

To further examine charge compensation mechanisms, hard X-ray absorption (XAS) spectroscopy at Mn K-edge is applied for $Li_{1-x}Mn_{0.5}Ti_{0.5}S_2$ (**Figure 3b**). No change is found in absorption energy position on de-lithiation/re-lithiation. A minor change around the absorption peak top at 6547 eV for fully charged sample, and such change in an XAS profile is known to originate from changes in local environments for transition metal ions associated with Li extraction.[27] Note that similar results are found for $Li_{1-x}Mn_{0.5}Ti_{0.5}S_2$ as shown in **Supporting Figure S5.** This finding suggests that Mn ion is not responsible for charge compensation, and activation of anionic redox is expected. Soft X-ray photoelectron spectroscopy (SOXPES) was used to measure electronic structures for S ions on electrochemical cycles. For SOXPES measurement, Quantera SXM (ULVAC-PHI) equipped with an Al-Kα X-ray source (1486.6 eV) was used. SOXPES spectra of $LiMn_{0.5}Ti_{0.5}S_2$ before and after

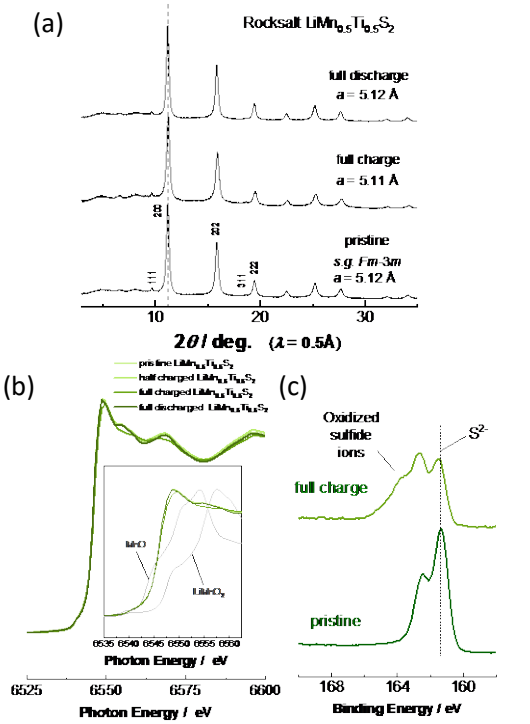

Figure 3. (a) Structural evolution of rocksalt $Li_{1-x}Mn_{0.5}Ti_{0.5}S_2$ measured by *ex-situ* XRD study. (b) Changes in Mn K-edge XAS spectra of rocksalt $Li_{1-x}Mn_{0.5}Ti_{0.5}S_2$, the data of MnO and $LiMnO_2$ are also plotted in the inset, and SOXPES spectra of the same samples are also shown in (c).

charge are shown in **Figure 3**c. A peak from sulfide ions is found at 161 eV, which is clearly weakened after charge. Instead, new peaks appear above 162 eV, which would be assigned as new chemical species formed by oxidation of sulfide ions. Similar finding is observed by SOXPES study for $Li_{1.25-x}Ti_{0.75}S_2$.[9] These results indicate that pure anionic redox is effectively used for charge compensation. Further studies of the origin of new peaks observed by SOXPES are in progress in our group, and the results will be reported elsewhere.

Higher solubility of metal sulfides hinders its use for practical applications with aprotic electrolyte solution. Therefore, $LiMn_{0.5}Ti_{0.5}S_2$ with the rocksalt structure was tested with solid polymer electrolyte without solvent.[28] To prepare the solid polymer electrolyte membrane, poly(ethylene oxide) (PEO) (Wako Chemicals, M_w: 3,600,000–4,000,000) and lithium bis(trifluoromethanesulfonyl)amide (LiTFSA) (Wako Chemicals) with a molar ratio of 15:1 are mixed in an agate mortar for 15 min in the glove box filled with argon. The obtained rough sheet film is placed between stainless steel plates. Then, the sheet was hot-pressed[28] at 100 °C for 60 min under 20 kN pressure. The mixture consisted of 70 wt% $LiMn_{0.5}Ti_{0.5}S_2$, 6 wt% poly(vinylidene fluoride), 6 wt% poly(ethylene oxide), 8 wt% lithium bis(trifluoromethanesulfonyl)imide, 10 wt% acetylene black, was mixed with NMP, and casted on Al foil used as current collector. After drying of casted composite layer, the membrane and composite layer were hot-pressed at 50 °C under the pressure of 5 kN for 5 min to make the better interface. Then, lithium foil (100 μm thickness) is attached on the membrane in the Ar-filled glove box. Finally, a solid-state polymer cell, Li | PEO/LiTFSA membrane | $LiMn_{0.5}Ti_{0.5}S_2$ composite layer, were assembled as shown in **Figure 4a**. Charge/discharge curves of $LiMn_{0.5}Ti_{0.5}S_2$ with polymer electrolyte are shown in **Figure 4b**. The cells with polymer electrolyte without solvent deliver larger reversible capacities of 250 and 230 mA h g^{-1} at 10 and 30 mA g^{-1}, respectively. Similar reversible capacities are obtained with the cell with carbonate-based electrolyte solution (**Figure 2**). Moreover, much improved reversibility is achieved as shown in **Figure 4c** because of the suppression of dissolution of sulfide-based electrode materials.

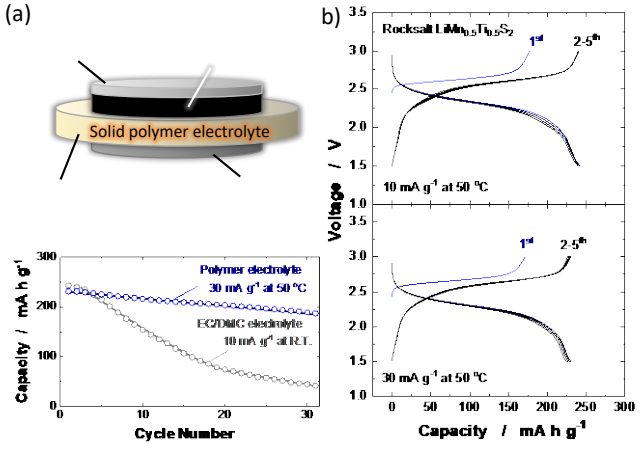

Figure 4. (a) A schematic illustration of a solid-state polymer cell used in this study. Mass loading of rocksalt $LiMn_{0.5}Ti_{0.5}S_2$ ranges from 2.4 to 2.7 mg/cm². (b) Galvanostatic charge/discharge curves of $Li_{1-x}Mn_{0.5}Ti_{0.5}S_2$ with polymer electrolyte at 50 °C, and capacity retention of the polymer cell compared with the result with carbonate-based electrolyte solution is shown (c).

In this study, $LiMe_{0.5}Ti_{0.5}S_2$ (*Me* = Fe^{2+}, Mn^{2+}, and Mg^{2+}) are synthesized and evaluated as positive electrode materials for

Li-ion batteries. Electrode reversibility of metal sulfides is significantly influenced by the presence of transition metal ions associated with electronic conductivity, and metal sulfides with the disordered structure shows better performance as electrode materials. Although metal sulfides suffer from the degradation of cyclability because of higher solubility to carbonate-based electrolyte solution, electrode reversibility with anionic redox is effectively improved by the use of polymer-based solid electrolyte. Comparative study of metal sulfides with oxides contributes further development of lithium insertion materials, leading to the further development of Li-ion batteries with higher energy density with reversible anionic redox.

Acknowledgments

NY acknowledges the partial support from JSPS, Grant-in-Aid for Scientific Research (Grant Numbers 19H05816, 21H04698, and 21K18815), and MEXT program "Elements Strategy Initiative to Form Core Research Center (JPMXP0112101003)", MEXT; Ministry of Education Culture, Sports, Science and Technology, Japan. The synchrotron X-ray absorption work was done under the approval of the Photon Factory Program Advisory Committee (Proposal No. 2021G039). The synchrotron radiation experiments were performed at the BL19B2 of SPring-8 with the approval of the Japan Synchrotron Radiation Research Institute (JASRI) (Proposal No. 2021B1722).

ASSOCIATED CONTENT

SEM images and capacity retention of cation-disordered rocksalt and cation-ordered layered Li*Me*$_{0.5}$Ti$_{0.5}$S$_2$ (*Me* = Fe^{2+}, Mn^{2+}, and Mg^{2+}), comparison of impedance for LiMn$_{0.5}$Ti$_{0.5}$S$_2$ and LiMg$_{0.5}$Ti$_{0.5}$S$_2$, impedance of rocksalt and layered LiMn$_{0.5}$Ti$_{0.5}$S$_2$, XRD patterns and Fe K-edge XAS spectra of rocksalt Li$_{1-x}$Fe$_{0.5}$Ti$_{0.5}$S$_2$, XRD patterns of rocksalt Li$_{1-x}$Mn$_{0.5}$Ti$_{0.5}$S$_2$.

AUTHOR INFORMATION

Corresponding Author

*e-mail: yabuuchi-naoaki-pw@ynu.ac.jp

References

(1) Kim, U.-H.; Park, G.-T.; Conlin, P.; Ashburn, N.; Cho, K.; Yu, Y.-S.; Shapiro, D. A.; Maglia, F.; Kim, S.-J.; Lamp, P.; Yoon, C. S.; Sun, Y.-K. Cation ordered Ni-rich layered cathode for ultra-long battery life, *Energy Environ. Sci.* **2021**.

(2) Geng, C.; Liu, A.; Dahn, J. R. Impact of Aluminum Added to Ni-Based Positive Electrode Materials by Dry Particle Fusion, *Chem. Mater.* **2020**, *32*, 6097-6104.

(3) Ikeda, N.; Konuma, I.; Rajendra, H. B.; Aida, T.; Yabuuchi, N. Why is the O3 to O1 phase transition hindered in LiNiO2 on full delithiation?, *J. Mater. Chem. A* **2021**, *9*, 15963-15967.

(4) Vaalma, C.; Buchholz, D.; Weil, M.; Passerini, S. A cost and resource analysis of sodium-ion batteries, *Nature Rev. Mater.* **2018**, *3*, 18013.

(5) Nakanishi, A.; Ueno, K.; Watanabe, D.; Ugata, Y.; Matsumae, Y.; Liu, J.; Thomas, M. L.; Dokko, K.; Watanabe, M. Sulfolane-Based Highly Concentrated Electrolytes of Lithium Bis(trifluoromethanesulfonyl)amide: Ionic Transport, Li-Ion Coordination, and Li–S Battery Performance, *J. Phys. Chem. C* **2019**, *123*, 14229-14238.

(6) Hagen, M.; Hanselmann, D.; Ahlbrecht, K.; Maça, R.; Gerber, D.; Tübke, J. Lithium–Sulfur Cells: The Gap between the State-of-the-Art and the Requirements for High Energy Battery Cells, *Adv. Energy Mater.* **2015**, *5*, 1401986.

(7) Whittingham, M. S. Electrical Energy Storage and Intercalation Chemistry, *Science* **1976**, *192*, 1126-1127.

(8) Sakuda, A.; Takeuchi, T.; Okamura, K.; Kobayashi, H.; Sakaebe, H.; Tatsumi, K.; Ogumi, Z. Rock-salt-type lithium metal sulphides as novel positive-electrode materials, *Scientific Reports* **2014**, *4*, 4883.

(9) Flamary-Mespoulie, F.; Boulineau, A.; Martinez, H.; Suchomel, M. R.; Delmas, C.; Pecquenard, B.; Le Cras, F. Lithium-rich layered titanium sulfides: Cobalt- and Nickel-free high capacity cathode materials for lithium-ion batteries, *Energy Storage Mater.* **2020**, *26*, 213-222.

(10) Saha, S.; Assat, G.; Sougrati, M. T.; Foix, D.; Li, H.; Vergnet, J.; Turi, S.; Ha, Y.; Yang, W.; Cabana, J.; Rousse, G.; Abakumov, A. M.; Tarascon, J.-M. Exploring the bottlenecks of anionic redox in Li-rich layered sulfides, *Nat. Energy* **2019**, *4*, 977-987.

(11) Takada, K.; Kitami, Y.; Inada, T.; Kajiyama, A.; Kouguchi, M.; Kondo, S.; Watanabe, M.; Tabuchi, M. Electrochemical Reduction of Li[sub 2]FeS[sub 2] in Solid Electrolyte, *J. Electrochem. Soc.* **2001**, *148*, A1085.

(12) Tatsumisago, M.; Nagao, M.; Hayashi, A. Recent development of sulfide solid electrolytes and interfacial modification for all-solid-state rechargeable lithium batteries, *Journal of Asian Ceramic Societies* **2013**, *1*, 17-25.

(13) Sato, T.; Sato, K.; Zhao, W.; Kajiya, Y.; Yabuuchi, N. Metastable and nanosize cation-disordered rocksalt-type oxides: revisit of stoichiometric LiMnO2 and NaMnO2, *J. Mater. Chem. A* **2018**, *6*, 13943-13951.

(14) Sawamura, M.; Kobayakawa, S.; Kikkawa, J.; Sharma, N.; Goonetilleke, D.; Rawal, A.; Shimada, N.; Yamamoto, K.; Yamamoto, R.; Zhou, Y.; Uchimoto, Y.; Nakanishi, K.; Mitsuhara, K.; Ohara, K.; Park, J.; Byon, H. R.; Koga, H.; Okoshi, M.; Ohta, T.; Yabuuchi, N. Nanostructured LiMnO2 with Li3PO4 Integrated at the Atomic Scale for High-Energy Electrode Materials with Reversible Anionic Redox, *ACS Cent. Sci.* **2020**, *6*, 2326-2338.

(15) Yabuuchi, N. Material Design Concept of Lithium-Excess Electrode Materials with Rocksalt-Related Structures for Rechargeable Non-Aqueous Batteries, *Chem. Rec.* **2019**, *19*, 690-707.

(16) Campéon, B. D. L.; Yabuuchi, N. Fundamentals of metal oxide/oxyfluoride electrodes for Li-/Na-ion batteries, *Chem. Phys. Rev.* **2021**, *2*, 041306.

(17) Assat, G.; Tarascon, J.-M. Fundamental understanding and practical challenges of anionic redox activity in Li-ion batteries, *Nat. Energy* **2018**, *3*, 373-386.

(18) Marchini, F.; Saha, S.; Alves Dalla Corte, D.; Tarascon, J. M. Li-Rich Layered Sulfide as Cathode Active Materials in All-Solid-State Li–Metal Batteries, *ACS Appl. Mater. Interfaces* **2020**, *12*, 15145-15154.

(19) Kobayashi, Y.; Sawamura, M.; Kondo, S.; Harada, M.; Noda, Y.; Nakayama, M.; Kobayakawa, S.; Zhao, W.; Nakao, A.; Yasui, A.; Rajendra, H. B.; Yamanaka, K.; Ohta, T.; Yabuuchi, N. Activation and stabilization mechanisms of anionic redox for Li storage applications: Joint experimental and theoretical study on Li2TiO3–LiMnO2 binary system, *Mater. Today* **2020**, *37*, 43-55.

(20) Momma, K.; Izumi, F. VESTA 3 for three-dimensional visualization of crystal, volumetric and morphology data, *J. Appl. Crystallogr.* **2011**, *44*, 1272-1276.

(21) Tsuchiya, Y.; Glushenkov, A. M.; Yabuuchi, N. Effect of Nanosizing on Reversible Sodium Storage in a NaCrO2 Electrode, *ACS Appl. Nano Mater.* **2018**, *1*, 364-370.

(22) Kitajou, A.; Tanaka, K.; Miki, H.; Koga, H.; Okajima, T.; Okada, S. Improvement of Cathode Properties by Lithium Excess in Disordered Rocksalt Li2+2xMn1-xTi1-xO4, *Electrochemistry* **2016**, *84*, 597-600.

(23) Qi, R.; CampÉOn, B. D. L.; Konuma, I.; Sato, Y.; Kaneda, Y.; Kondo, M.; Yabuuchi, N. Metastable and Nanosized Li1.2Nb0.2V0.6O2 for High-Energy Li-ion Batteries, *Electrochemistry* **2022**, *in-press*.
(24) Nakajima, M.; Yabuuchi, N. Lithium-Excess Cation-Disordered Rocksalt-Type Oxide with Nanoscale Phase Segregation: Li1.25Nb0.25V0.5O2, *Chem. Mater.* **2017**, *29*, 6927-6935.
(25) Sakuda, A.; Ohara, K.; Kawaguchi, T.; Fukuda, K.; Nakanishi, K.; Arai, H.; Uchimoto, Y.; Ohta, T.; Matsubara, E.; Ogumi, Z.; Kuratani, K.; Kobayashi, H.; Shikano, M.; Takeuchi, T.; Sakaebe, H. A Reversible Rocksalt to Amorphous Phase Transition Involving Anion Redox, *Scientific Reports* **2018**, *8*, 15086.
(26) Abdellahi, A.; Urban, A.; Dacek, S.; Ceder, G. Understanding the Effect of Cation Disorder on the Voltage Profile of Lithium Transition-Metal Oxides, *Chem. Mater.* **2016**, *28*, 5373-5383.
(27) Kubobuchi, K.; Mogi, M.; Matsumoto, M.; Baba, T.; Yogi, C.; Sato, C.; Yamamoto, T.; Mizoguchi, T.; Imai, H. A valence state evaluation of a positive electrode material in an Li-ion battery with first-principles K- and L-edge XANES spectral simulations and resonance photoelectron spectroscopy, *J. Appl. Phys.* **2016**, *120*, 142125.
(28) Wang, L.; Li, X.; Yang, W. Enhancement of electrochemical properties of hot-pressed poly(ethylene oxide)-based nanocomposite polymer electrolyte films for all-solid-state lithium polymer batteries, *Electrochim. Acta* **2010**, *55*, 1895-1899.

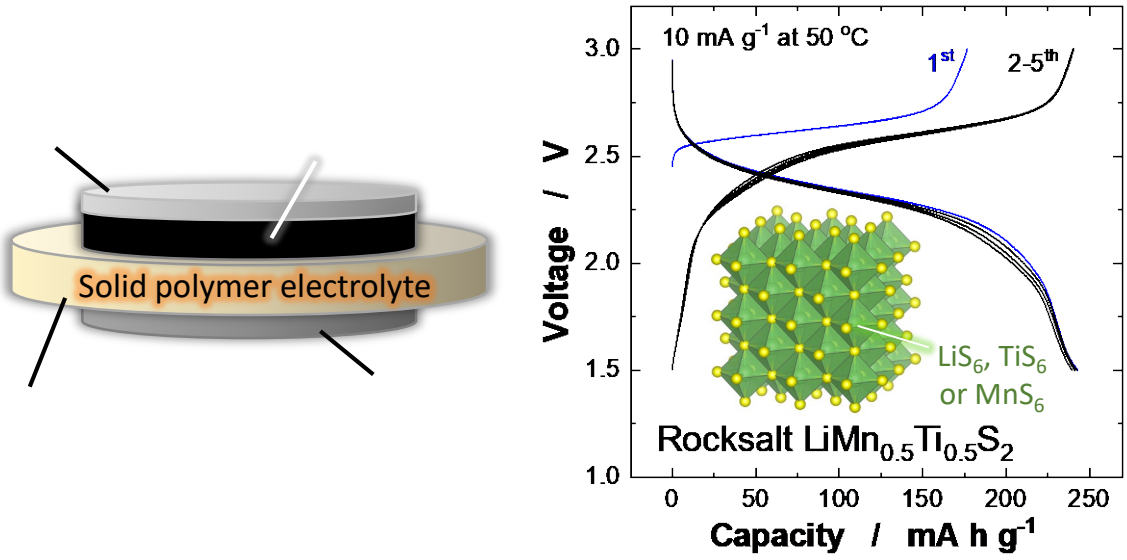

Insert Table of Contents artwork here